coatings

MDPI

Article

Chemical Vapor Deposition of Tantalum Carbide in the $TaBr_5$–CCl_4–Cd System

Tibor Krenicky [1,*], Oleg Y. Goncharov [2], Jiri Kuchar [3], Irina V. Sapegina [2], Jan Kudlacek [3], Ravil R. Faizullin [4], Alexander I. Korshunov [2] and Daniel Cerny [3]

1 Department of Technical Systems Design and Monitoring, Faculty of Manufacturing Technologies with a seat in Presov, Technical University of Kosice, Bayerova 1, 080 01 Presov, Slovakia
2 FSBIS Udmurt Federal Research Center, Ural Branch of the Russian Academy of Sciences, T. Baramzinoy Str. 34, 426067 Izhevsk, Russia; oniolaf@gmail.com (O.Y.G.); kai@udman.ru (A.I.K.)
3 Department of Manufacturing Technology, Faculty of Mechanical Engineering, Czech Technical University in Prague, Technicka 4, 16000 Prague, Czech Republic; jiri.kuchar@fs.cvut.cz (J.K.); jan.kudlacek@fs.cvut.cz (J.K.); d.cerny@fs.cvut.cz (D.C.)
4 Scientific Production Association Protective Coatings, LLC, Lenina Pr. 142-116, Moscow Region, 142100 Podolsk, Russia; fajzu55@gmail.com
* Correspondence: tibor.krenicky@tuke.sk; Tel.: +421-55-602-6337

Abstract: The tantalum carbide coatings were deposited on substrates made of 12Kh18N10T steel, ZhC6 alloy, and molybdenum by reduction of $TaBr_5$ and CCl_4 vapors with cadmium vapors at temperatures of 950–1000 K. The average deposition rate of coatings on molybdenum was ~5 μm/h, on ZhC6 alloy was ~6 μm/h, and on 12Kh18N10T steel was ~8 μm/h. The coatings were formed as columnar grains on the substrate surface and as a diffuse layer in the substrate material. The surface layers contained mainly tantalum monocarbide TaC_y (y = 0.72–0.86) and a small fraction of tantalum. The coatings on the surface of ZhC6 alloy and 12Kh18N10T steel flaked off with increasing thickness, which was due to different thermal expansion of the coating and substrate, as well as concentration inhomogeneity and phase transitions in the substrate material during coating deposition and during the heating and cooling processes.

Keywords: chemical vapor deposition; carbide tantalum coating; diffuse layers

Citation: Krenicky, T.; Goncharov, O.Y.; Kuchar, J.; Sapegina, I.V.; Kudlacek, J.; Faizullin, R.R.; Korshunov, A.I.; Cerny, D. Chemical Vapor Deposition of Tantalum Carbide in the $TaBr_5$–CCl_4–Cd System. *Coatings* **2024**, *14*, 547. https://doi.org/10.3390/coatings14050547

Academic Editor: Cheng Zhang

Received: 11 March 2024
Revised: 22 April 2024
Accepted: 23 April 2024
Published: 27 April 2024

1. Introduction

Various non-stoichiometric carbides can be formed in the Ta-C system [1–3], among which Ta_2C, TaC, and zeta-phase ζ-Ta_4C_3 [4,5] are the most studied. Monocarbide TaC may contain from 37 to 50 at.% carbon (at a temperature of 3749 K), β-Ta_2C may contain from 26 to 35 at.% carbon at a temperature of 3047 K, and zeta-phase ζ-Ta_4C_3 may contain from 38 to 39 at.% carbon.

Tantalum monocarbide TaC has a high melting point of 4270 K, is resistant to thermal shocks, corrosion, chemicals [6], oxidation, and ablation [7], and therefore can be used with various high-temperature materials. For example, ceramic composites TaC/C [8] and TaC/SiC [9] are used for high-temperature heavy-duty applications. TaC coatings are used as diffuse barrier layers [10,11]. TaC–C–Al composites containing 10–20 at.% Ta and 6–7 at.% Al are innovative high-temperature wear-resistant coatings with excellent antifriction properties [12,13].

Ta_2C and Ta_4C_3 carbides are frequently formed as by-products in the preparation of tantalum monocarbide. For example, some carbide phases are formed in coatings where there are concentration gradients of elements (carbon and tantalum). The melting point of Ta_2C carbide is ~3600 K; it is more resistant to oxidation [14] and has higher ductility [15] than TaC. The presence of zeta-phase ζ-Ta_4C_3 in the mixture of tantalum carbide increases the fracture toughness and improves the mechanical strength of the material [16,17].

Tantalum carbide coatings may be obtained by various methods [18–27]. For example, the coating is deposited on the substrate in the form of solutions of metal-containing complex compounds with polymers [18,19], which are then dried and pyrolyzed (at T = 623–873 K). After that, carbothermal synthesis is performed (at T = 873–1473 K and a pressure not more than 10^{-4} Pa). The disadvantages of this method are non-uniform distribution of the gel over a surface and shrinkage of the coating during drying and annealing, which results in non-uniform thickness and density of the coatings. In addition, expensive organometallic chemicals are required to produce coatings. To reduce the cost of tantalum carbide coatings production, TaC powder was sintered with organic binders at temperatures above 2300 K, which made it possible to form dense carbide layers (up to 200 μm) [20,21]. However, this method of coating is not applicable for parts with complex shapes, as well as substrates with a melting point of 2300 K and below.

Tantalum carbide coatings were deposited on parts with complex shapes by organometallic compounds pyrolysis at 623–1573 K [22,23]. In addition, tantalum carbides were prepared by plasma atomic layer deposition (PEALD) from organometallic compounds at temperatures around 673 K [24]. The high cost and polymerization ability of organometallic compounds limit their application because, for example, polymerization products can block evaporators and gas pipelines.

Usually, a mixture of reagents containing tantalum source, carbon source, and hydrogen is used for chemical vapor deposition of tantalum carbides. For example, tantalum carbide coatings were deposited from a mixture of $TaCl_5$, CH_4, H_2, and He on a substrate heated up to 1493–1653 K [25] according to the following reactions:

$$TaCl_5 + CH_4 + 1/2\ H_2 = TaC + 5\ HCl, \quad (1)$$

$$2\ TaCl_5 + CH_4 + 3\ H_2 = Ta_2C + 10\ HCl. \quad (2)$$

The temperature of carbide deposition can be reduced to about 1323 ÷ 1423 K by reducing the pressure in the reaction chamber (to ~10^4 Pa) [26]. Replacement of methane CH_4 by ethane C_2H_6 results in an increase in the rate of carbide deposition. Thus, tantalum carbides were deposited from a mixture of $TaCl_5$, C_2H_6, and H_2 at a temperature of 1373 ÷ 1573 K and pressure of ~10^4 Pa [19,27].

There are some constraints for deposition of tantalum carbide from a $TaCl_5$–C_3H_6–H_2 (or $TaCl_5$–CH_4–H_2) mixture. The melting temperature of substrate should not be lower than the coating deposition temperature. An equipment used for deposition should have excellent corrosion resistance to chlorine and hydrogen chloride, as well as resistance to hydrogen brittleness. In addition, hydrogen and hydrocarbons should be used with extreme caution due to their flammability and explosion hazard.

The heat of tantalum bromide $TaBr_5$ formation (−143 kcal/mol) is lower than that of chloride $TaCl_5$ (−205 kcal/mol) [28]. Therefore, to reduce the deposition temperature in Reactions (1) and (2), it is reasonable to use $TaBr_5$ (instead of $TaCl_5$), which is volatile at relatively low temperatures (vapor pressure is ~10 torr at 473 K). In addition, the corrosion of metals in bromine compounds is less than in chlorine compounds. Instead of hydrocarbons in Reactions (1) and (2), it is convenient to use carbon tetrachloride CCl_4, which is a volatile fire-safe liquid that easily dissociates upon heating. Hydrogen in Reactions (1) and (2) can be replaced by vapors of reducing metals such as zinc [29], calcium [30], cadmium [31,32], magnesium, sodium, and potassium. Cadmium is a convenient reducing agent because it is volatile at relatively low temperatures (saturated vapor pressure is 1333 Pa at 763 K) [33]). Cadmium bromides and chlorides are also easily volatile at temperatures above 850 K, and therefore, their co-deposition with carbides is not possible. Thus, the $TaBr_5$–CCl_4–Cd system could be promising for the deposition of tantalum carbides according to the following reactions:

$$TaBr_5 + CCl_4 + 4.5\ Cd = TaC + 2\ CdCl_2 + 5/2\ CdBr_2, \quad (3)$$

$$2\ TaBr_5 + CCl_4 + 10\ Cd = Ta_2C + 5\ CdCl_2 + 5\ CdBr_2. \quad (4)$$

The optimal parameters of the deposition of tantalum carbides in the $TaBr_5$–CCl_4–Cd–He system were evaluated in the temperature range T = 673 ÷ 1673 K, pressure P = 1.01 × 10^5 Pa, and the ratio of elements in the reaction mixture Ta/(Ta + C) = 0.01 ÷ 0.909; Cd/(Cd + hal) = 0 ÷ 0.952 (hal = Cl + Br) [34]. It was found that pure tantalum carbides could be deposited at temperatures above T = 840 K, while lower temperatures of cadmium chloride impurities will be deposited. Monocarbide TaC_y (y = 0.815 ÷ 1) can be formed at T = 840 ÷ 1100 K, and at 973 K, the maximum fraction of tantalum conversion to monocarbide ~0.6 can be achieved at a slight excess of tantalum in the reaction mixture Ta/C = 1.35 and 0.6 < Cd/hal < 9. Carbide $Ta_{2-z}C$ (z = 0.085 ÷ 0.199) can be formed at T = 960 ÷ 1070 K, and at 973 K, the maximum fraction of tantalum conversion to $Ta_{2-z}C$ is ~0.6 and can be achieved at ratios of Ta/C = 3 and 0.5 < Cd/hal < 9. The maximum fraction of tantalum conversion to carbides of ~0.9 can be achieved with two-phase compositions TaC + C, which is achieved at the following ratios: 0.1 < Ta/C < 1 and 0.6 < Cd/hal < 9.

The present work investigates the processes of chemical vapor deposition of tantalum carbides by reduction of tantalum bromide (and CCl_4) with cadmium vapor on substrates made of 12X18H10T steel, ZhC6 superalloy and molybdenum. The coatings were deposited on equipment that we developed specifically to enable metal vapor reduction processes [31,32].

2. Materials and Methods

2.1. Coating Deposition Equipment

Tantalum carbide coatings in the $TaBr_5$–CCl_4–Cd–He system were deposited in a CVD reactor of our own design [35], with separate delivery of reagents to the reaction zone using inert carrier gas streams (Figure 1). The carrier gas was saturated with reagent vapors in the lower and upper evaporator chambers [36]. The lower evaporator was used to supply cadmium vapor at temperatures above 723 K. The upper evaporator was used to supply tantalum bromide vapor at temperatures above 423 K. The content of reagents in the carrier gas flows was set by the temperature of the evaporators. The content of CCl_4 vapor was set using a temperature-controlled evaporator [37].

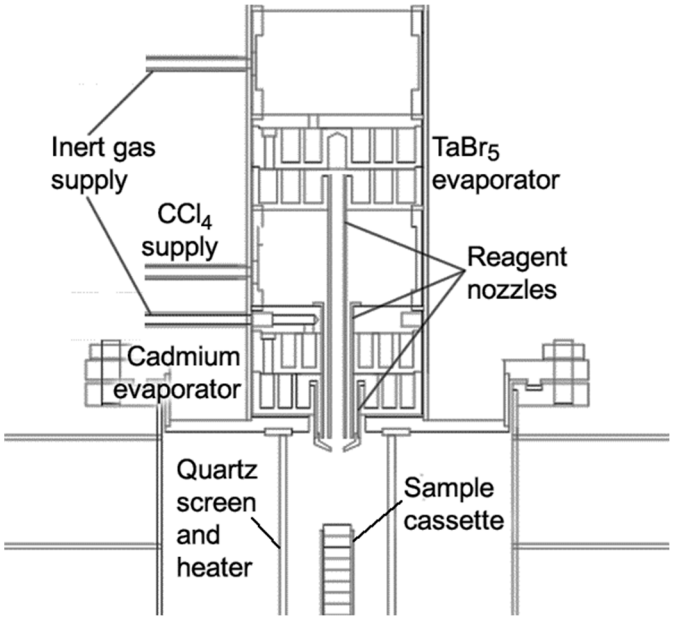

Figure 1. Reagent supply to the CVD reactor.

All reagents were delivered into the reaction chamber through separate channels, mixed in the vicinity above the sample and reacted, resulting in the precipitation of tantalum carbide. To heat samples and reagents, resistive heating was used (reagent heaters are not shown in Figure 1).

2.2. Sample Preparation and Coating Conditions

The coatings were deposited on flat polished samples (substrates) with a diameter of 12 mm, made of molybdenum (99.7 wt.%), 12Kh18N10T steel (Fe67Cr18Ni11Mn2Ti0.8Si0.8 Cu0.23C0.12S0.02P0.03 wt.%), nickel alloy ZhC6 (Ni59Cr11Co9W9Al6Ti2Mo2Nb1 (C, Si, Mn, Zr, B, Y) 1 wt.%). In addition, samples made of 12Kh18N10T steel and Mo with a previously deposited tantalum coating were used [31]. The samples were installed in a special cassette [38] inside the reactor and pushed out from the holder tube as required. The distance from the nozzle cut-off to the sample was set at no more than 30 mm. Increasing the distance from the nozzle to the sample increases the possibility of homogeneous reactions in the gas phase with the formation of powders.

The concentration of reagent vapor in the evaporators, c_i (mol/m^3), was calculated by the Clapeyron–Mendeleev equation:

$$c_i = p_i/RT, \quad (5)$$

where p_i, Pa, is the partial vapor pressure at the evaporator temperature T, K.

The amount of reagent delivered to the reaction chamber, C_i (mol/h), was determined by the equation:

$$C_i = c_i \cdot G_i, \quad (6)$$

where G_i, m^3/h, is the gas flow rate in the evaporator.

The conditions of coatings deposition at deposition temperature of T_D = 950–1000 K are given in Table 1. The ratios of reagents for TaC and Ta2C deposition were chosen according to calculations [34] so that the cadmium content in the reaction mixture was minimized.

Table 1. Conditions for the deposition of tantalum carbides.

Deposition Parameters [1]	Reagents		
	$TaBr_5$	Cd	CCl_4
p_i, Pa	533–933	1066–1600	1466–1866
Gi, ml/s	2–5	3–8	0.3–1
$C_i \times 10^{-3}$, mol/h	1.7–2.5	2.4–4.6	0.6–3.1
t, h		0.5–4	
Ta/Cd/C		1/(1 ÷ 2)/(0.5 ÷ 1.2)	

[1] Deposition parameters: p_i, G_i, C_i are the parameters of Equations (1) and (2); t is the deposition time; *Ta/Cd/C* is the molar ratio of elements in the reaction mixture.

2.3. Methods of Coating Analysis

To investigate the crystalline structure of coatings, X-ray diffractometers DRON-6 and DRON-3 were used (Bourevestnik, JSC, Saint Petersburg, Russia). X-ray diffraction patterns were made in monochromatized Cu Kα and Co Kα radiations; angular range 20–100 deg.; scan step 0.1 deg.; counting time per data point 10 s. X-ray focusing was made using the Bragg–Brentano method.

Layer-by-layer analysis of elements content and coating thickness measurements were performed using Glow Discharge Optical Emission Spectrometer (GDOES) GDA 650 HR (Spectruma Analytik GmbH, Hof, Germany), with detection limits from 1 ppm to 50 ppm and a depth resolution of about 50 nm.

The composition and chemical structure of the surface layers of the coating were analyzed by X-ray photoelectron spectroscopy (XPS) using SPECS spectrometer with excitation of the photoelectron spectrum by Mg Kα (E = 1253.6 eV). The Casa XPS software ver 2.3.26 (Casa Software Ltd., Teignmouth, UK) was used to process the spectral data. The relative error of element concentration determination is ±3%. XPS analysis was performed at depths of ~5 nm and ~25 nm with argon etching at a rate of ~1 nm/min. The chemical state of elements was analyzed by XPS spectra of core electron levels with reference data [39] and reference spectra. The 4f XPS spectrum of metallic tantalum was obtained and used as a reference spectrum.

To investigate the microstructure of the coating surface, we used scanning electron microscope (SEM), a Thermo Fisher Scientific Quattro S with an energy dispersive spectroscopy system based on EDAX spectrometer Octane Elect Plus EDS System (Thermo Fisher Scientific, Brno, Czech Republic).

3. Results and Discussion

3.1. Features of Tantalum Carbide Deposition at Early Stages (Up to 30 min)

Tantalum carbide coatings were deposited on the surface of all prepared substrates. At a deposition time of 30 min, the thickness of coatings reached from 1 to 2 µm. The tantalum carbide coatings on the molybdenum samples had a homogeneous microstructure and inherited scratches that were formed by polishing the substrate (Figure 2). The intensity of the X-ray diffraction peaks from the tantalum carbide coating (Figure 3) are much smaller than the peaks from the molybdenum substrate. This is because the tantalum carbide coatings on molybdenum were thinner than coatings on other types of substrates. In addition, in the spectra of characteristic radiations of elements for the area in Figure 2, the most intense lines corresponded to the characteristic radiation of molybdenum, and the lines of coating elements (tantalum and carbon) were much less intense.

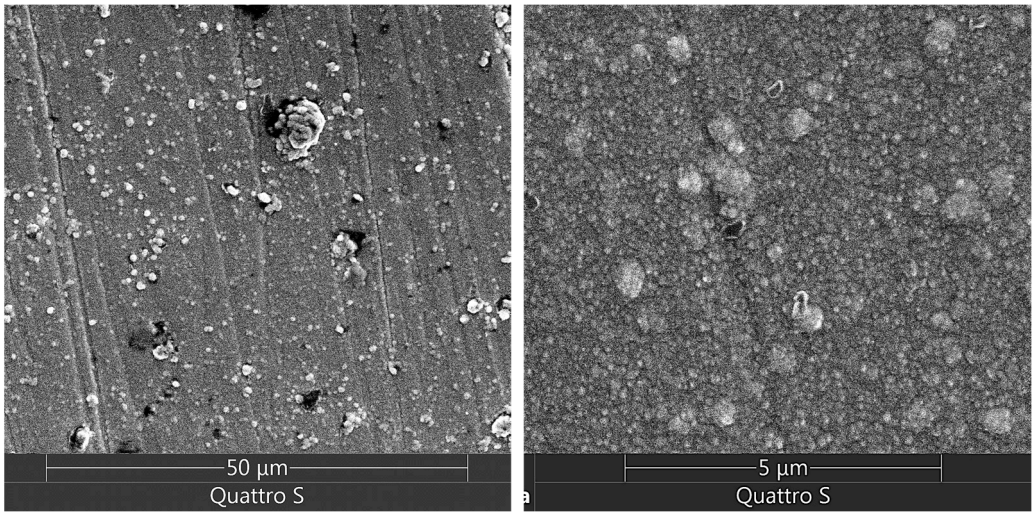

Figure 2. SEM image of the tantalum carbide coating on molybdenum substrate (30 min) with more detailed view on the right.

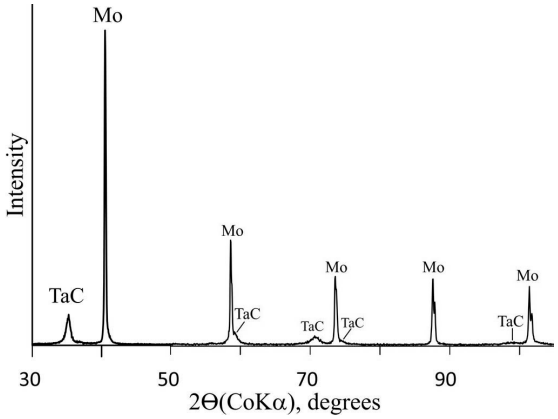

Figure 3. X-ray diffraction pattern of the coating on molybdenum substrate (30 min).

In the C1s XPS spectrum of molybdenum coatings, there were peaks with binding energies of 283 and 284.8 eV (Figure 4a). The peak with a binding energy of 283 eV corresponds to carbon–metal compounds in carbide-like compounds, and the second peak

with a binding energy of 284.8 eV corresponds to C–C bonds in graphite-like structures [40]. For the spectrum of Ta4f7/2 at a coating depth of 25 nm, the maximum peak is at 23 eV, whereas for the tantalum reference sample, this value is 21.8 eV (Figure 4b). This difference indicates tantalum carbide formation [39,41]. Analysis of the C1s and Ta4f7/2 spectra shows that tantalum carbide formed at a depth of 25 nm has non-stoichiometric composition TaC_{1-x} with $x \leq 0.17$. Simultaneously, a very small fraction of carbon has C–C bonds.

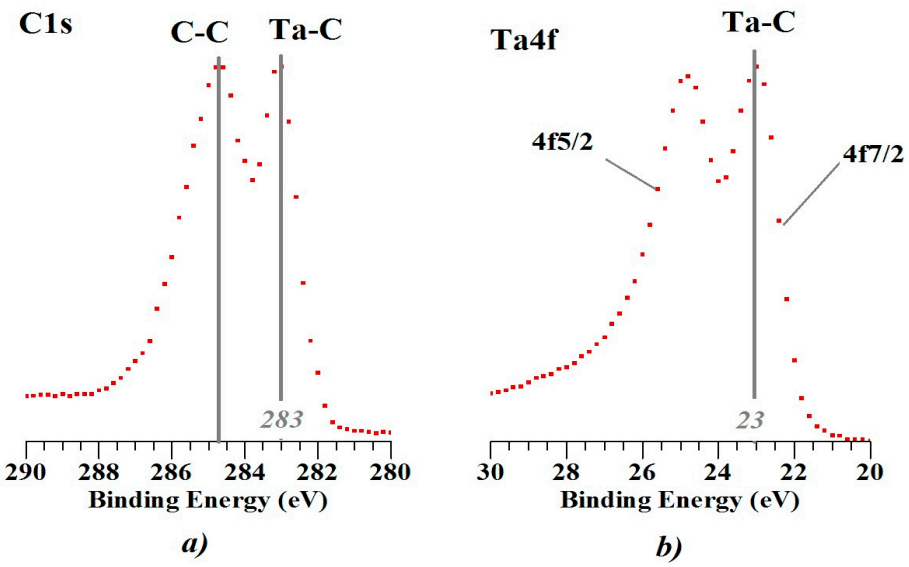

Figure 4. XPS spectra of (**a**) C1s and (**b**) Ta4f for coatings at a depth of 25 nm.

Analysis of the XPS spectra also revealed that at a depth of ~25 nm the tantalum/carbon ratio is ~43/45, and at a depth of ~5 nm the tantalum/carbon ratio is ~26/53 (Table 2). A small increase in the carbon content in the top layers of the coating up to ~5 nm is due to the features of the experiment. Toward the end of the experiment, the flow CCl_4 vapor to the reaction chamber was stopped last, which resulted in a small excess decomposition of CCl_4 vapor on the coating surface. Analysis of XPS spectra also showed that the content of oxygen impurities decreased significantly from the surface to the depth of the coatings (Table 2). That is, the oxygen impurities in the surface layers of the coatings were introduced mainly in the examination of the coatings and much less during deposition.

Table 2. Percentage element composition of the coating deposited on different substrates at depths of 5 and 25 nm (in parentheses).

Sample/Deposition Time (min)	Ta, at.%	C, at.%	Cr, at.%	Fe, at.%	Ni, at.%	O, at.%
Mo/30	26 (43)	53 (45)				21 (12)
12Kh18N10T/30	18 (36)	74 (54)	0 (2)			8 (8)
ZhC6/30	18 (35)	61 (45)		2 (4)		19 (16)
Mo/60	39 (44)	47 (48)	3 (4)	3 (1)		7 (3)
ZhC6/60	43 (51)	44 (39)			5 (6)	8 (3)
ZhC6/240	30 (46)	57 (46)	2 (2)	1 (1)	1 (1)	8 (4)

The coatings deposited for 30 min on ZhC6 substrates were thicker than those on molybdenum. Also, no polishing marks were observed on the coatings (Figure 5), and the intensity of the X-ray peaks of the coating material was higher than that of the substrate material (Figure 6). On the energy dispersive spectra, the peaks of Ta and C were also more intense than those of the substrate elements. Randomly placed conglomerates of crystallites ranging in size from 0.2 to 1.5 μm were observed on the surface of the coatings (Figure 5).

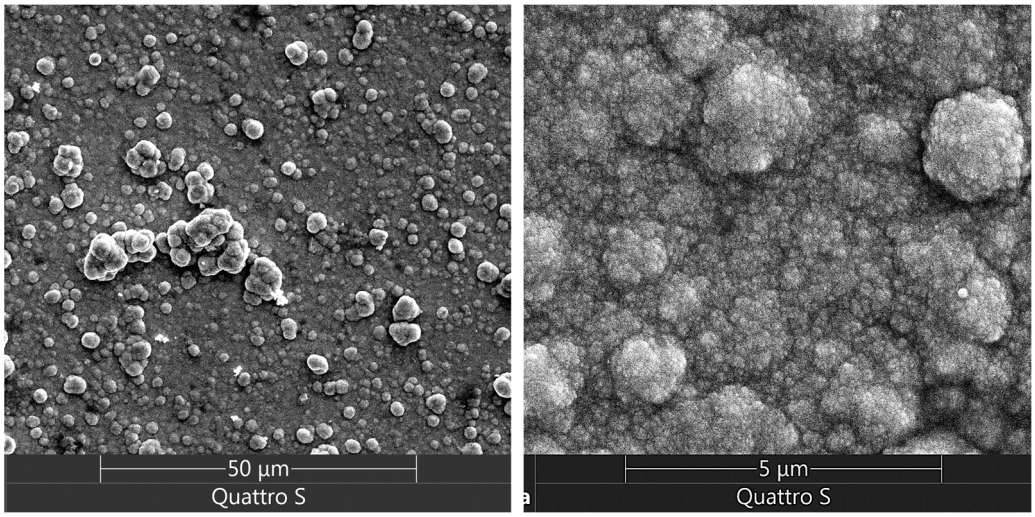

Figure 5. SEM image of the tantalum carbide coating on ZhC6 substrate (30 min) with more detailed view on the right.

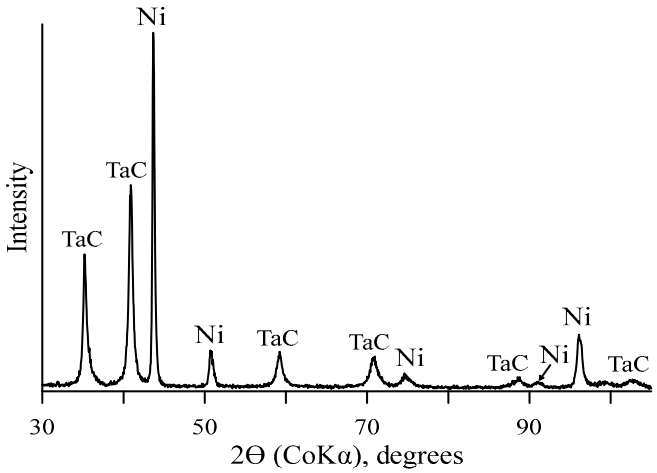

Figure 6. X-ray diffraction analysis of the coating on ZhC6 substrate (30 min).

The analysis of XPS spectra of C1s and Ta4f7/2 coatings from ZhC6 alloy shows that at a depth of 5 nm, carbon forms mainly C–C bonds, and C–Ta bonds are much less. The number of C–C bonds decreases with depth. The tantalum/carbon ratio at a depth of ~5 nm is ~1/3.3, and at a depth of 25 nm it is ~1/1.3 (Table 2). At a 25 nm depth, the carbide composition corresponds to that of TaC_{1-x} with $x \leq 0.17$, as for the coating on molybdenum. The increase in the number of C–C bonds in the top layers of the coating (up to 5 nm) is due to the fact that the CCl_4 flux is switched off last at the end of deposition, as for coatings on molybdenum substrate. In addition, the content of oxygen impurity in the upper layers of the coating (up to 5 nm) increases due to the adsorption of oxygen on the surface during the coating analysis process.

Tantalum carbide coatings deposited on 12X18N10T steel for 30 min were thicker than coatings deposited on molybdenum, but slightly thinner than coatings deposited on ZhC6 alloy. The surface of the coatings showed no traces of substrate polishing (Figure 7), and the intensity of the TaC X-ray diffraction peaks was comparable to that of the substrate material (Figure 8). The coating surface is a homogeneous layer of conglomerates of crystallites, with a diameter of ~0.5 µm each (Figure 7), located normal to the surface.

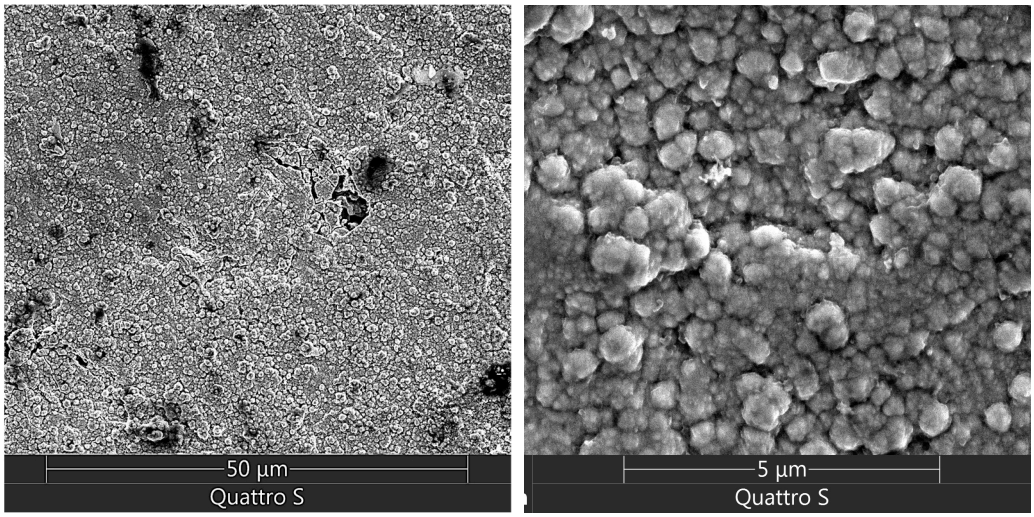

Figure 7. SEM image of the tantalum carbide coating on 12Kh18N10T substrate (30 min) with more detailed view on the right.

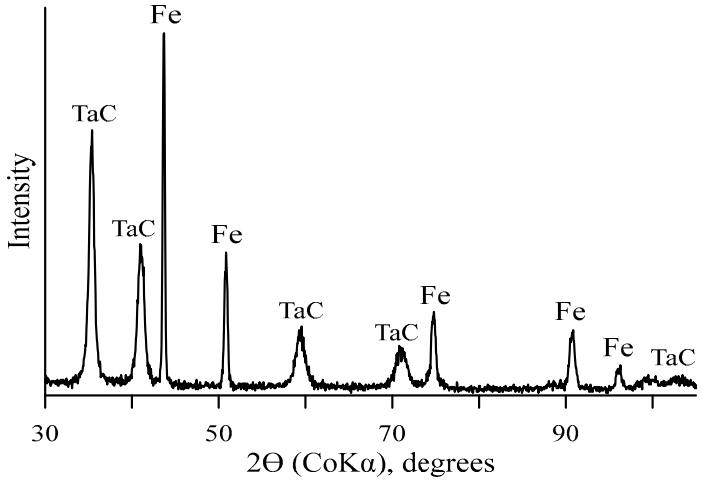

Figure 8. X-ray diffraction analysis of the coating on 12Kh18N10T substrate (30 min).

Analysis of the C1s XPS spectra of the coatings on 12Kh18N10T showed that there are more C–C bonds than C–Ta bonds in the layers at depths of 5 and 25 nm (Figure 8). The number of C–C bonds decreases, and the number of C–Ta bonds increases with depth. For tantalum carbide TaC_{1-x}, the stoichiometry was determined from the spectrum of Ta4f7/2 and was $x \leq 0.17$ at a depth of 25 nm, which coincides with the stoichiometry of coatings deposited on molybdenum and ZhC6. The tantalum/carbon ratio is ~1/4 at a depth of ~5 nm, and ~3/2 at a depth of 25 nm (Table 2). In addition, oxygen impurities up to 8 at.% and chromium impurities up to 2 at.% were detected in the surface layers of the coatings, which appeared there during deposition and analysis of the coatings (Table 2).

3.2. Deposition of Tantalum Carbide Coatings over 30 min

The coatings deposited on molybdenum for 1 h had a thickness of about 4 µm (Figure 9) and uniform fine-crystalline structure. Substrate polishing marks are noticed on the coatings, and the X-ray diffraction spectra contain peaks from both tantalum monocarbide and the substrate material (Figure 9). The ratio of the intensities of the (002) and (111) TaC X-ray peaks is ~2.3 (standard one is ~0.6), which indicates the formation of texture in the coating.

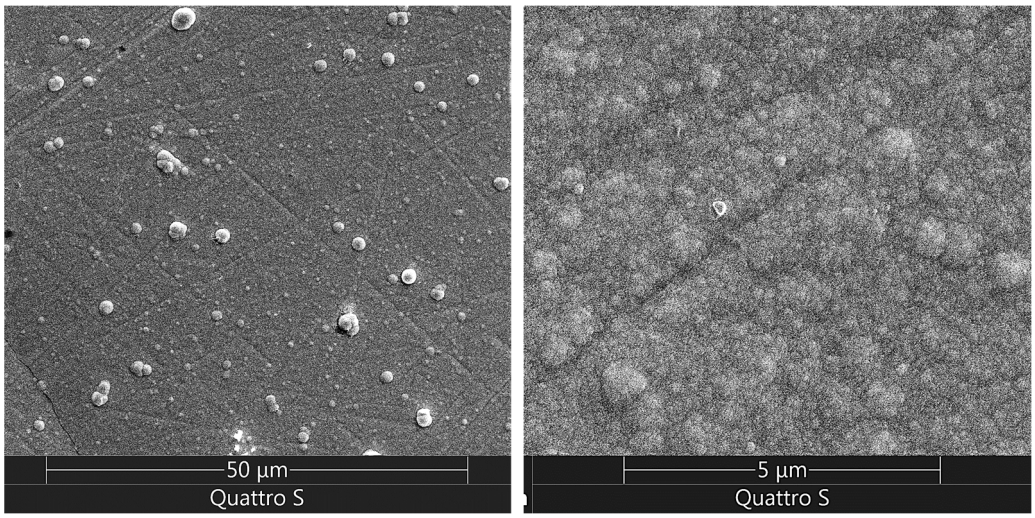

Figure 9. SEM image of the tantalum carbide coating on molybdenum substrate (60 min) with more detailed view on the right.

The analysis of XPS C1s and Ta4f7/2 spectra demonstrated that the Ta/C ratio in the coating at a depth of 5 nm is higher than in a similar layer of the coating that was deposited on molybdenum for 30 min (Figure 10). This means that the Ta/C ratio on the coating surface increases with deposition time. Already at a depth of 25 nm, the Ta/C ratio is close to 1, as in the coating deposited on molybdenum for 30 min. Despite this, at a depth of 25 nm, tantalum carbide is non-stoichiometric TaC_{1-x} with $x \leq 0.17$ since part of the carbon is in the form of C–C bonds. The impurity content of the coating decreases with depth, hence most of the impurities are adsorbed after deposition.

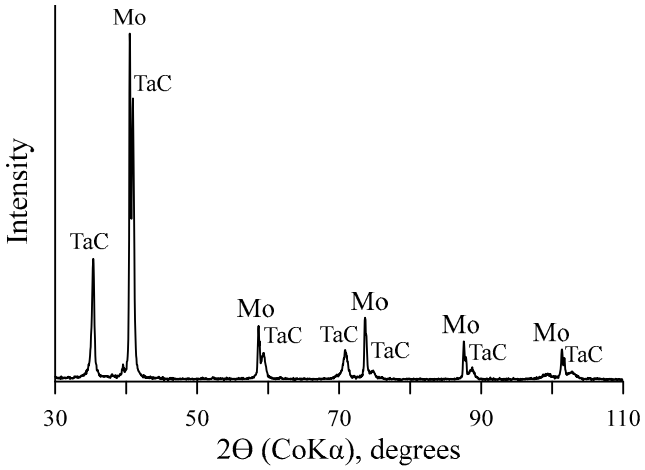

Figure 10. X-ray diffraction analysis of the carbide coating on the molybdenum substrate (60 min).

When the deposition time was increased up to two hours, columnar crystals growing perpendicularly to the substrate were observed on the coating surfaces (Figure 11). This behavior is typical for CVD coatings at relatively low temperatures [42]. The crystals are equiaxed within the axes parallel to the deposition surface and are spheroidal in the growth direction. This normal crystallite growth was observed on all substrates used, with coating deposition times longer than 30 min. The growth of columnar crystals is driven by geometric selection [43]. The randomly oriented small grains are gradually dissolved by the coalescence and grain coarsening, and the grains grow preferentially in a direction perpendicular to the surface of the coating, resulting in the formation of columnar crystals with the same orientation.

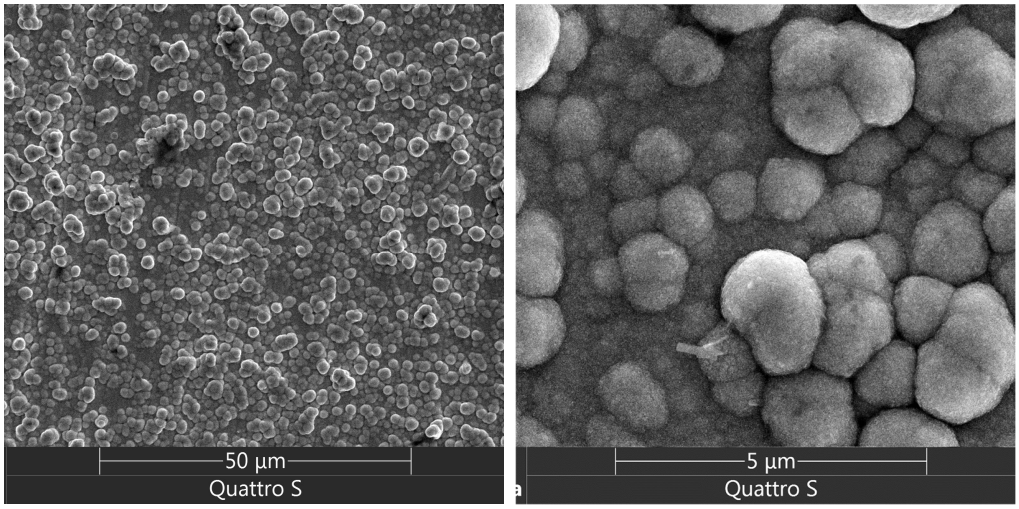

Figure 11. SEM image of the tantalum carbide coating on molybdenum substrate (120 min) with more detailed view on the right.

For the molybdenum coatings, analysis of the XPS spectra showed that near the surface and at a depth of 25 nm, the Ta/C ratio is approximately 1, and the tantalum carbide has a composition of TaC_{1-x} with $x \leq 0.17$. The layer-by-layer analysis of the elemental composition (Figure 12) demonstrates that the total thickness of the carbide layer is about 10 µm, and for TaC_{1-x}, the average non-stoichiometry is $x \sim 0.5$. In addition, there is a diffuse layer with tantalum and carbon in a molybdenum matrix at a depth of 6 to 10 µm between the coating and the substrate.

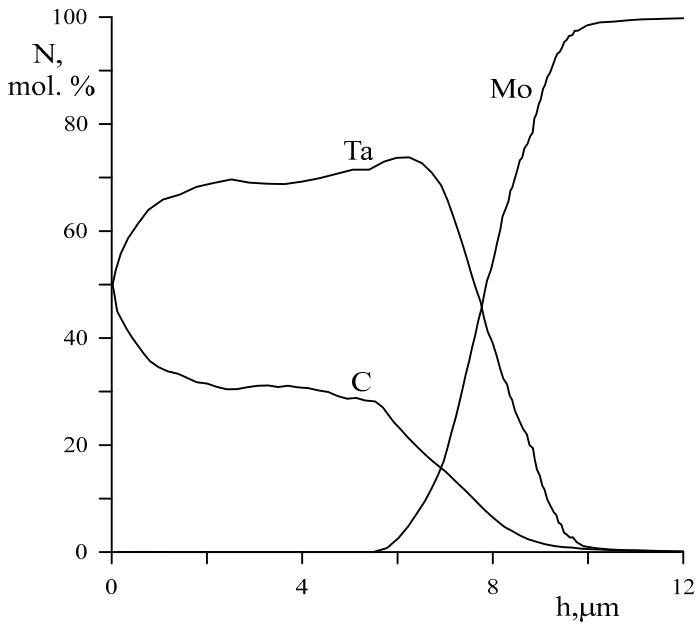

Figure 12. Layer-by-layer analysis of the element content of the coating on molybdenum (120 min).

The ZhC6 alloy coatings deposited for 1 h were also formed as columnar crystals oriented perpendicularly to the substrate, with a spheroidal top in the growth direction (Figure 13). The thickness of these coatings was about 4 µm, there were no marks of substrate polishing on the coatings, and both tantalum monocarbide peaks and less intense peaks corresponding to the substrate were present in the X-ray spectrum (Figure 14).

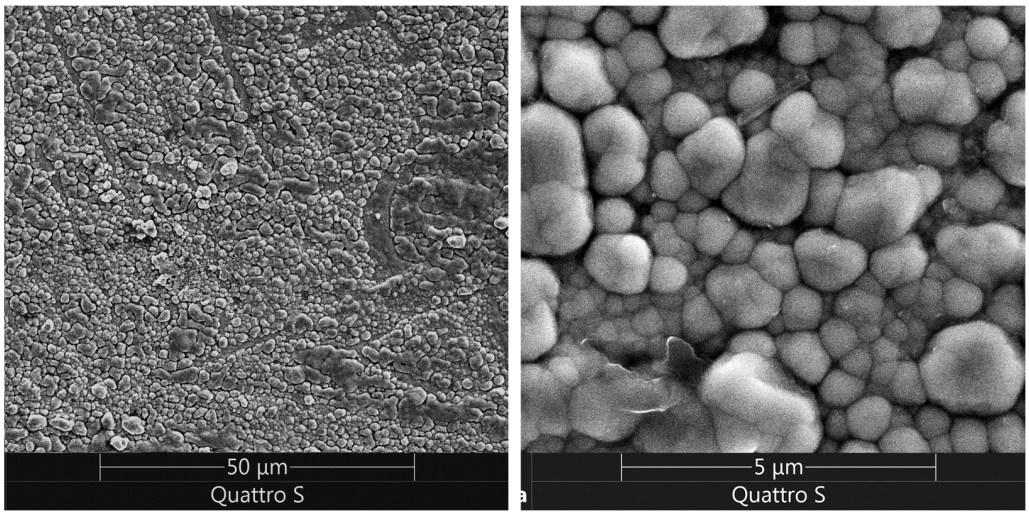

Figure 13. SEM image of the tantalum carbide coating on ZhC6 substrate (60 min) with more detailed view on the right.

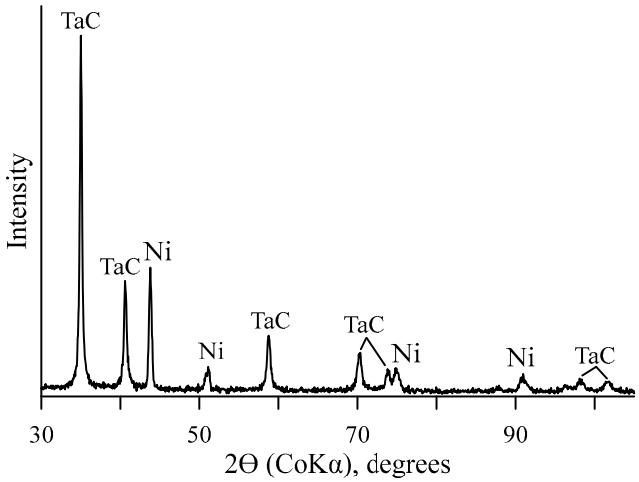

Figure 14. X-ray diffraction analysis of the carbide coating on the ZhC6 substrate (60 min).

The analysis of XPS spectra of the coatings on ZhC6 alloy at depths of 5 and 25 nm demonstrates the same patterns as for the coatings deposited on Mo. The tantalum/carbon ratio increases slightly with increasing depth (Table 2), and at a depth of 25 nm, the tantalum carbide has the composition TaC_{1-x} with $x \leq 0.17$. In the upper layers of the coating, we observed up to 6 at.% of nickel, which apparently diffused from the substrate.

When the deposition coating time on the ZhC6 alloy was increased to 4 h, flaking of the upper coating layers was observed while the lower coating layers remained intact (Figure 15).

X-ray diffraction analysis of the coatings demonstrates presence of tantalum monocarbide (Figure 16). The coating is relatively thick, so only weak reflections from the substrate are visible in the X-ray diffraction pattern. The thickness of the coatings was about 13 µm, of which 8 µm is the carbide layer and 5 µm is the diffuse layer (Figure 15). Layer-by-layer analysis showed that near the surface, the coating composition was close to stoichiometric tantalum monocarbide (Figure 17). The tantalum content in the carbide decreased with depth down to 5 µm. Between 5 and 8 µm, we observed a slight increase in tantalum content of the coating, but the carbide composition was still non-stoichiometric.

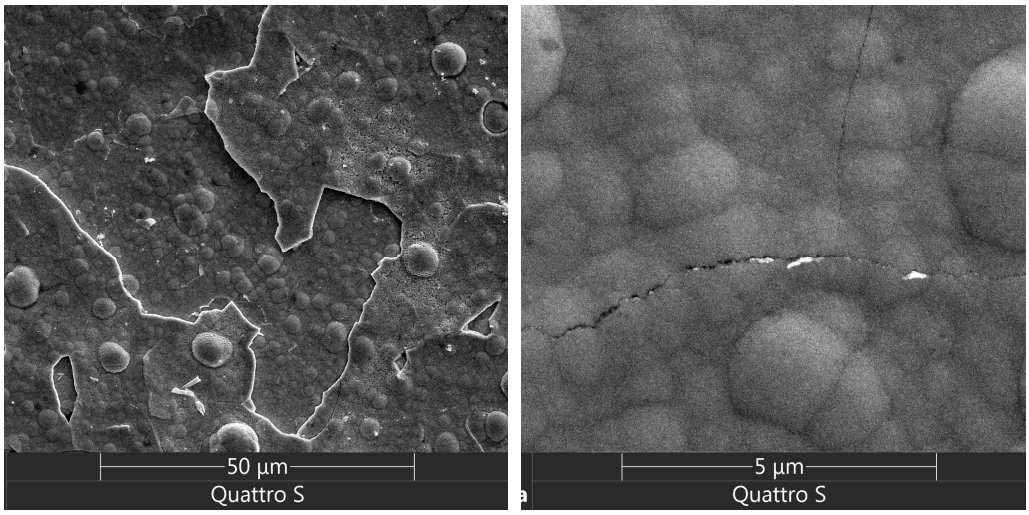

Figure 15. SEM image of the tantalum carbide coating on ZhC6 substrate (4 h) with more detailed view on the right.

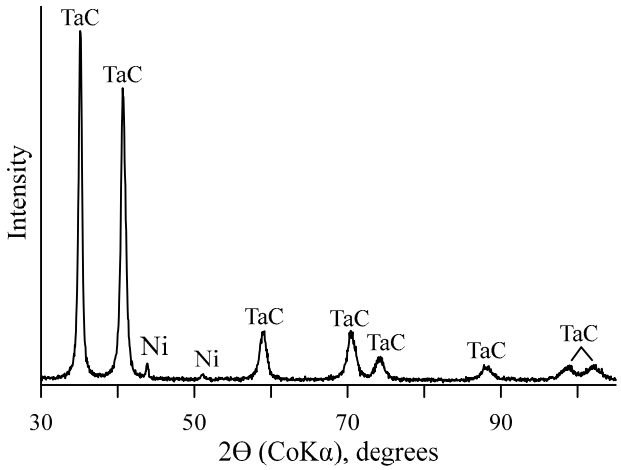

Figure 16. X-ray diffraction analysis of the carbide coating on ZhC6 substrate (240 min).

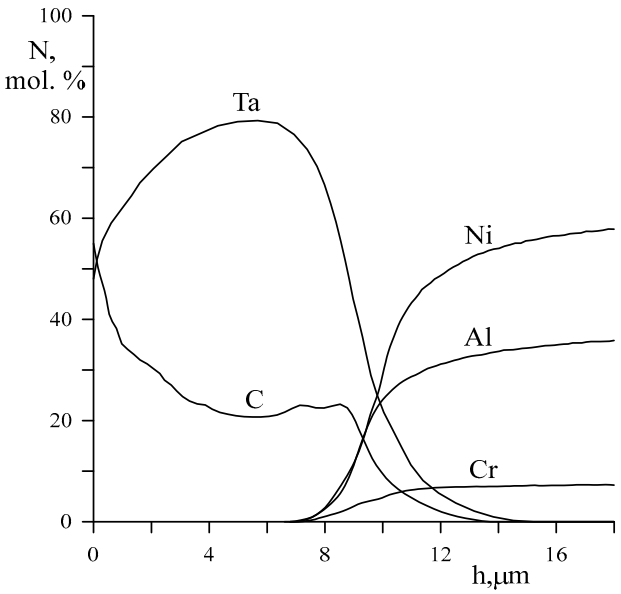

Figure 17. Layer-by-layer analysis of the element content of the coating on the ZhC6 (120 min).

The coatings deposited on 12Kh18N10T steel within one hour (Figure 18) are similar to those on ZhC6 alloy (Figure 13). The thickness of the coatings is about 5 μm, and the coatings consist of two phases of TaC and Ta_2C (Figure 19). The substrate had a dual-phase structure composed of γFe and αFe (Figure 19).

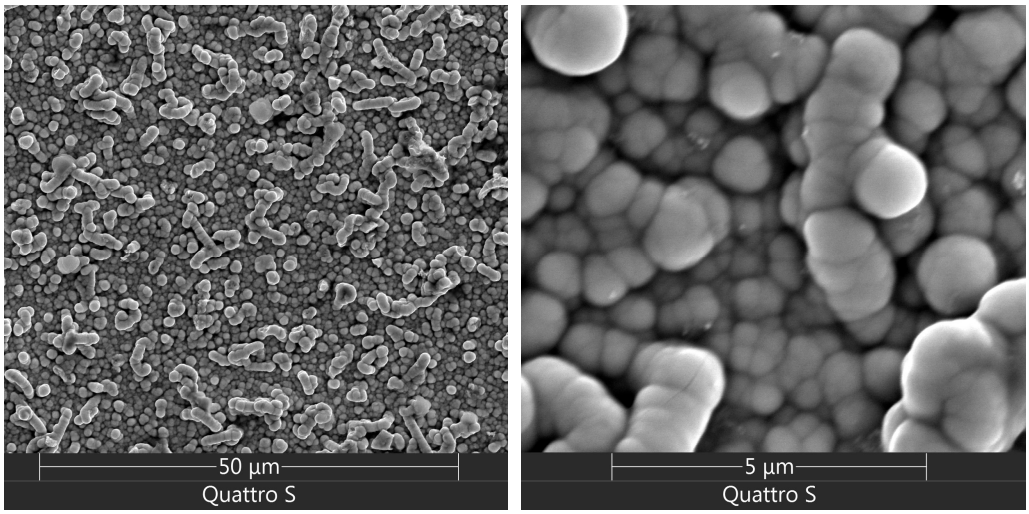

Figure 18. SEM image of the tantalum carbide coating on 12Kh18N10T steel (60 min) with more detailed view on the right.

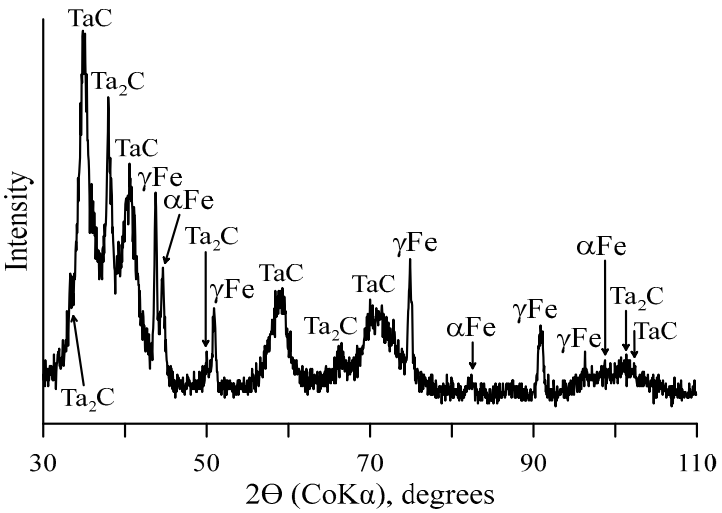

Figure 19. X-ray diffraction analysis of the carbide coating on the 12Kh18N10T substrate (60 min).

When the deposition time was prolonged by up to two hours, the coatings cracked (Figure 20), similar to the coatings deposited on ZhC6 for 4 h (Figure 15). The thickness of the coatings was ~17 μm, of which ~8 μm was in the carbide layer and ~9 μm in the diffuse layer (Figure 21). The composition of TaC in the carbide layer was non-stoichiometric even at the surface. The coatings contained iron impurities up to ~5% in the carbide layer.

As a rule, flaking and damage of the coating is the result of internal stresses. One of the reasons for internal stress formation is the different thermal expansion of the substrate and coating layers. Therefore, the coefficients of thermal expansion (CTE) for substrates and coatings (at temperatures of 295 to 1000 K) were compared in order to estimate the possibility of coating failure.

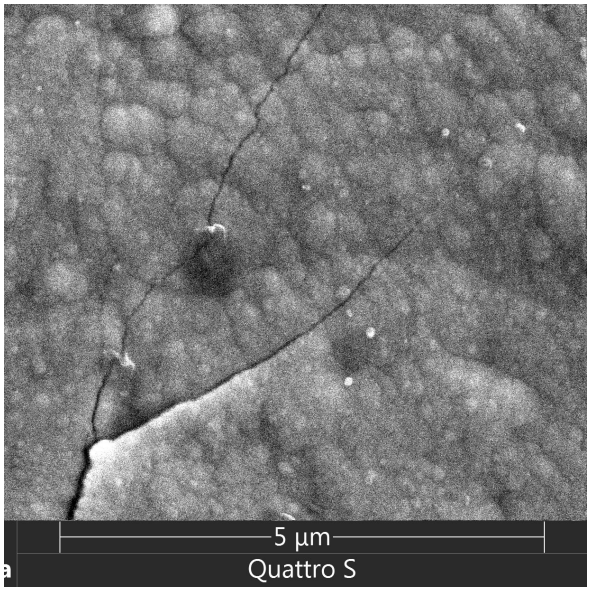

Figure 20. SEM image of the tantalum carbide coating on 12Kh18N10T steel (120 min).

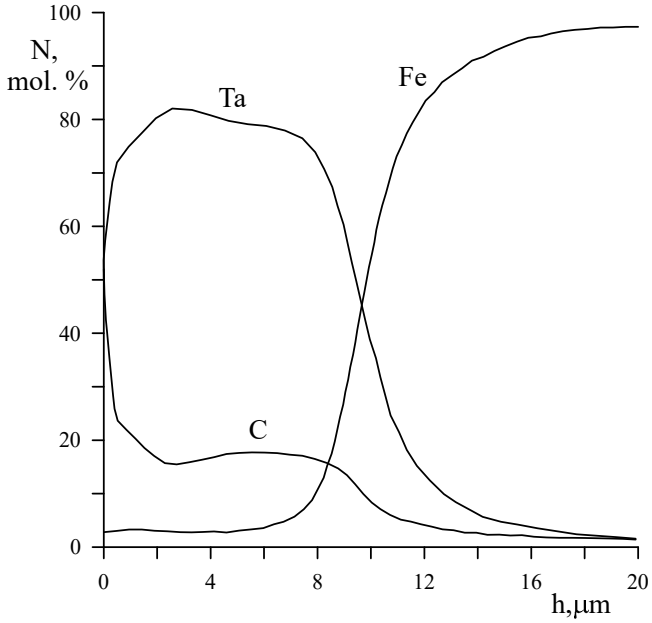

Figure 21. Layer-by-layer analysis of the element content of the coating on the 12Kh18N10T steel (120 min).

The coefficient of thermal expansion of TaC_y increases with increasing "y" and is equal to 6.04, 6.37, 6.96 × 10^{-6} K^{-1} for $TaC_{0.789}$, $TaC_{0.912}$, and $TaC_{0.997}$, respectively [44]. The CTE of TaC films is 6.7–8.2 × 10^{6} K^{-1} [45]. The CTE of Ta_2C films is 7.2 × 10^{-6} K^{-1} [46]. The coefficient of thermal expansion of molybdenum is 5.8 × 10^{-6} K^{-1} [47], which is close to the coefficient of thermal expansion of tantalum carbides. That is why relatively thick layers of tantalum carbide deposited on molybdenum did not flake off. The coefficient of thermal expansion of ZhC6 alloy is 15 × 10^{-6} K^{-1} [48], which is approximately twice that of tantalum carbides. Therefore, internal stresses increase with the increase in the thickness of ZhC6 coating, and this results in flaking of coatings thicker than 12 µm after four hours of deposition (Figure 15). The coefficient of thermal expansion of 12Kh18N10T steel (an analogue of ANSI321) is even higher: CTE = 18.6 × 10^{-6} K^{-1} [49,50]. In addition, the αFe/γFe phase ratio in 12Kh18N10T steel varies with the temperatures of coating deposition and subsequent cooling [51]. Thus, the significant difference in the CTEs between the 12Kh18N10T substrate and a coating, as well as α-γ phase transformations

in the steels, results in the formation of cracks in coatings thicker than 12 μm within two hours after the start of deposition (Figure 20) rather than four hours, as with the ZhC6 alloy substrate.

During the coating process, there is an induction period when nucleation of deposition products begins to form on surface defects [43,52]. The induction period is characterized by a low deposition rate. As the nucleation layer forms, the observed deposition rate increases in response to the growth of the solid phase interfaces. The growing coating slowly covers the nucleation centers on the substrate, resulting in a decrease in the observed deposition rate. Another reason for deposition deceleration is the decrease in phase interface area, caused by the competitive growth of grains that are oriented perpendicularly to the substrate surface.

At the temperature of carbide deposition, molybdenum's surface has relatively few point defects [53]. The low concentration of surface defects results in a low initial rate of coating formation and a relatively long induction period. Therefore, the initial deposition rate of tantalum carbide on molybdenum was lower than the rate of deposition on ZhC6 alloy and 12Kh18N10T steel. For ZhC6 alloy, the main defects are dislocations at γ'/γ phase interface and produced carbide particles of MeC type where (Me = Ti, Mo, W, etc.) [54]. The formation of defects on austenitic steels, such as 12Kh18N10T, has been studied [55,56]. Segregation of solid γ-solution occurs in steels, and at temperatures above T = 673 K, concentration inhomogeneities with high chromium content and α-phase particles are formed. In the range between 723 K and 948 K, a reverse α-γ transformation takes place that results in the formation of reticular dislocation structure in austenite and a slight decrease in steel volume. In addition, at temperatures of 673–973 K, there is a precipitation of carbide and intermetallic phase. The existence of different surface defects in 12Kh18N10T steel seems to cause an increase in coating thickening and the formation of a diffuse zone in the substrate, as well as iron diffusion in the coating.

Tantalum monocarbide TaC_y composition may vary from y = 0.6 to y = 1 with an unchanged cubic crystalline structure [3]. To estimate the value of "y", one may use tantalum monocarbide lattice constant a as a function of "y" [57]:

$$a(y, 0) = a_0 + a_1 y + a_2 y^2, \quad (7)$$

where a_0 = 4.1630 Å, a_1 = 0.4675 Å, and a_2 = −0.1750 Å.

Lattice constants and "y" evaluation results for deposited tantalum carbides obtained by Equation (7) are summarized in Table 3. The "y" value stays within a range of 0.72–0.86, which is close to the 0.83 value obtained by XPS methods at a depth of 25 nm for the same coatings.

Table 3. Lattice constants a and y values for tantalum carbide.

Substrate	a, Å	Non-Stoichiometry Degree	Ta/C GDA Estimation
12Kh18N10T/30	4.408	$TaC_{0.72}$	1/0.33
Mo/30	4.414	$TaC_{0.74}$	1/0.5
Mo/60	4.409	$TaC_{0.72}$	1/0.52
ZhC6/30	4.438	$TaC_{0.87}$	1/0.52
ZhC6/60	4.414	$TaC_{0.74}$	1/0.54
ZhC6/240	4.435	$TaC_{0.86}$	1/0.55

As per GDOES data, the average Ta/C ratio of coatings on various substrates is about 2/1 (Table 3), except for coatings on steel, for which the Ta/C ratio is 2/0.6. It means that the carbon content of the coating is closer to the Ta/C ratio in Ta_2C rather than to Ta/C ~0.6–1 in tantalum monocarbide [3]. As X-ray diffraction of a coating fails to determine if tantalum is present in any phase, it is likely that a part of it presents in the amorphous state.

It should be noted that the tantalum carbide deposition technique applied by us is similar to those techniques in which reaction mixtures based on $TaCl_5$–CH_4–H_2–Ar or

$TaCl_5$–C_3H_6–H_2–Ar were used [26,28,42]. All techniques produce a dense tantalum carbide coating with a columnar structure having a thickness of 10 μm within two hours at a deposition rate of ~5 μm/h. But only in our technique were such coatings deposited at temperatures of 950–1000 K and atmospheric pressure, whereas in [26,28,42], temperatures from 1323 to 1573 K and pressure reduction P ~10^4 Pa were required for carbide deposition.

4. Conclusions

We deposited tantalum carbides on 12Kh18N10T steel, ZhC6 alloy, and molybdenum through the reduction of $TaBr_5$ and CCl_4 vapors with cadmium vapors. The deposition was performed at 950–1000 K, within 30–240 min, in the flow reactor, with reagents fed in a carrier gas (helium) stream through the split channels, at a rate from 0.5×10^{-3} to 5×10^{-3} mol of a reagent per hour for each channel, with the reagent concentrations optimal for the formation of a mixture of TaC and Ta_2C carbide.

The coatings were deposited on the surface in the form of columnar grains, and additionally, a diffuse zone was formed in the substrate material. After two hours of deposition, the coating thickness on molybdenum was about 10 μm (4 μm diffuse layer), on ZhC6 alloy was 13 μm (5 μm diffuse layer), and on 12Kh18N10T steel was 17 μm (9 μm diffuse layer). The average rate of deposition was about 5 μm/h for molybdenum, 6 μm/h for ZhC6 alloy, and 8 μm/h for 12Kh18N10T steel. It seems that the difference in average rates of deposition is due to the different induction period time, which is dependent on substrate defect types and concentration.

X-ray diffraction revealed that the coatings on all substrates consisted mainly of $TaC_{0.72–0.86}$ (with an admixture of Ta_2C on steel). All coatings contained some part of tantalum, which was not determined by X-ray diffraction. According to XPS and GDOES data, near the coating surface the composition of tantalum carbide was close to stoichiometric, and at a depth of 25 nm, the composition of tantalum carbide was $TaC_{0.83}$.

The coatings on the molybdenum were deposited as dense layers. The coatings on the ZhC6 alloy partially flaked off after 4 h of deposition. The coatings on the 12Kh18N10T steel partially flaked off after 2 h of deposition. The cause of coating flaking was the difference between CTEs of the coating and the substrate, as well as in concentration inhomogeneities and phase transitions in the substrate material in the course of deposition during heating and cooling.

Author Contributions: Conceptualization, T.K., O.Y.G., J.K. (Jiri Kuchar) and R.R.F.; methodology, O.Y.G., J.K. (Jan Kudlacek) and R.R.F.; software, I.V.S., A.I.K. and D.C.; validation, T.K., J.K. (Jiri Kuchar) and R.R.F.; formal analysis, I.V.S., J.K. (Jan Kudlacek) and A.I.K.; investigation, O.Y.G. and I.V.S.; resources, T.K., O.Y.G., J.K. (Jiri Kuchar) and A.I.K.; data curation, T.K. and A.I.K.; writing—original draft preparation, O.Y.G. and R.R.F.; writing—review and editing, T.K., O.Y.G., J.K. (Jiri Kuchar) and A.I.K.; visualization, I.V.S., J.K. (Jan Kudlacek) and R.R.F.; supervision, T.K., O.Y.G., J.K. (Jiri Kuchar) and A.I.K.; project administration, T.K., O.Y.G., I.V.S. and J.K. (Jan Kudlacek); funding acquisition, T.K., O.Y.G., J.K. (Jiri Kuchar) and D.C. All authors have read and agreed to the published version of the manuscript.

Funding: This work was supported by the Slovak Ministry of Education, Science, Research and Sport within projects VEGA 1/0509/23 and KEGA 052TUKE-4/2024. The research was also supported by the project SGS22/156/OHK2/3T/12 "Influence of surface treatments on the quality of production technologies" and by the Russian Federation Ministry of Education and Science within projects No. RFMEFI 58214X0005, FUUE-2024-0007, and FUUE-2024-0010. The studies were performed using equipment of core shared research facilities of the "Center of physical and physical–chemical methods of analysis, investigations of properties and characteristics surface, nanostructures, materials and samples" of UdmFRC UrB RAS.

Institutional Review Board Statement: Not applicable.

Informed Consent Statement: Not applicable.

Data Availability Statement: The data presented in this study are available on request from the corresponding author. The data are not publicly available due to privacy reasons.

Conflicts of Interest: Ravil R. Faizullin was employed by the company Scientific Production Association Protective Coatings, LLC. The remaining authors declare that the research was conducted in the absence of any commercial or financial relationships that could be construed as a potential conflict of interest. The funders had no role in the design of the study; in the collection, analyses, or interpretation of data; in the writing of the manuscript; nor in the decision to publish the results.

References

1. Frisk, K.; Fernández Guillermet, A. Gibbs energy coupling of the phase diagram and thermo-chemistry in the tantalum-carbon system. *J. Alloys Compd.* **1996**, *238*, 167–179. [CrossRef]
2. Weisenberger, H.; Lengauer, W.; Ettmayer, P. Reactive diffusion and phase equilibria in the V-C, Nb-C, Ta-C and Ta-N systems. *Acta Mater.* **1998**, *46*, 651–666. [CrossRef]
3. Gusev, A.I.; Kurlov, A.S.; Lipatnikov, V.N. Atomic and vacancy ordering in carbide ζ-Ta_4C_{3-x} ($0.28 \leq x \leq 0.40$) and phase equilibria in the Ta–C system. *J. Solid State Chem.* **2007**, *180*, 3234–3246. [CrossRef]
4. Shabalin, I.L. Tantalum Carbides. In *Ultra-High Temperature Materials II*; Springer: Dordrecht, The Netherlands, 2019; pp. 9–144. [CrossRef]
5. Weinberger, R.C.; Thompson, G.B. A computational search for the zeta phase in the tantalum carbides. *J. Am. Ceram. Soc.* **2019**, *102*, 1454–1462. [CrossRef]
6. Shvab, S.A.; Egorov, F.F. Structure and Some Properties of Sintered Tantalum Carbide. *Powder Metall. Met. Ceram.* **1982**, *21*, 894–897. [CrossRef]
7. Li, G.D.; Xiong, X.; Huang, K.L. Ablation mechanism of TaC coating fabricated by chemical vapor deposition on carbon-carbon composites. *Trans. Nonferrous Met. Soc. China* **2009**, *19*, 689–695. [CrossRef]
8. Chen, Z.K.; Wu, Y.; Chen, Y.H.; Wang, H.R.; Zeng, Y.; Xiong, X. Preparation and oxidation behavior of Cf/C–TaC composites. *Mater. Chem. Phys.* **2020**, *254*, 123428. [CrossRef]
9. Liu, H.; Liu, L.; Ye, F.; Zhang, Z.; Zhou, Y. Microstructure and mechanical properties of the spark plasma sintered TaC/SiC composites: Effects of sintering temperatures. *J. Eur. Ceram. Soc.* **2012**, *32*, 3617–3625. [CrossRef]
10. Hong, T.E.; Kim, T.-H.; Jung, J.-H.; Kim, S.-H.; Kim, H. TaCx Thin Films Prepared by Atomic Layer Deposition as Diffusion Barriers for Cu Metallization. *J. Am. Ceram. Soc.* **2014**, *97*, 127–134. [CrossRef]
11. Wang, Z.; DelaCruz, S.; Tsai, D.-S.; Maboudian, R. W/TaC/SiC sandwich stack for high temperature applications. *Ceram. Int.* **2019**, *45*, 22292–22297. [CrossRef]
12. Zhao, Y.; Xu, J.; Peng, S. Synthesis and evaluation of TaC nanocrystalline coating with excellent wear resistance, corrosion resistance, and biocompatibility. *Ceram. Int.* **2021**, *47*, 20032–20044. [CrossRef]
13. Lv, D.; Chen, Z.; Xiong, X.; Wang, Y.; Sun, W.; Li, Z. Microstructure and tribological property of C-TaC coatings on graphite prepared by chemical vapor deposition. *Chin. J. Mater. Res.* **2016**, *30*, 690–696.
14. Desmaison-Brut, M.; Alexandre, N.; Desmaison, J. Comparison of the oxidation behaviour of two dense hot isostatically pressed tantalum carbide (TaC and Ta_2C). *Mater. J. Eur. Ceram. Soc.* **1997**, *17*, 1325–1334. [CrossRef]
15. Leon, N.D.; Wang, B.; Weinberger, C.R.; Thompson, G.B. Elevated Temperature Deformation Mechanisms in Ta_2C. *Microc. Microanal.* **2011**, *17*, 1898–1899. [CrossRef]
16. Hackett, K.; Verhoef, S.; Cutler, R.A.; Shetty, D.K. Phase constitution and mechanical properties of carbides in the Ta-C system. *J. Am. Ceram. Soc.* **2009**, *92*, 2404–2407. [CrossRef]
17. Sygnatowicz, M.; Cutler, R.A.; Shetty, D.K. ζ-Ta_4C_{3-x}: A High Fracture Toughness Carbide with Rising-Crack-Growth-Resistance (R-Curve) Behavior. *J. Am. Ceram. Soc.* **2015**, *98*, 2601–2608. [CrossRef]
18. Sevastyanov, V.G.; Simonenko, E.P.; Ignatov, N.A.; Ezhov, Y.S.; Kuznetsov, N.T. Low-temperature synthesis of TaC through transparent tantalum-carbon containing gel. *Inorg. Mater.* **2010**, *46*, 495–500. [CrossRef]
19. Kim, D.; Jeong, S.M.; Yoon, S.G.; Woo, C.H.; Kim, J.I.; Lee, H.-G.; Park, J.Y.; Kim, W.-J. Chemical vapor deposition of tantalum carbide from $TaCl_5$-C_3H_6-Ar-H_4 system. *J. Korean Ceram. Soc.* **2016**, *53*, 597–603. [CrossRef]
20. Nakamura, D.; Suzumura, A.; Shigetoh, K. Sintered tantalum carbide coatings on graphite substrates: Highly reliable protective coatings for bulk and epitaxial growth. *Appl. Phys. Lett.* **2015**, *106*, 082108. [CrossRef]
21. Nakamura, D.; Shigetoh, K.; Suzumura, A. Tantalum carbide coating via wet powder process: From slurry design to practical process tests. *J. Eur. Ceram. Soc.* **2017**, *37*, 1175–1185. [CrossRef]
22. Chang, Y.; Wu, J.; Chang, P.; Chiu, H. Chemical vapor deposition of tantalum carbide and carbonitride thin films from $Me_3CE{=}Ta(CH_2CMe_3)_3$ (E = CH, N). *J. Mater. Chem.* **2003**, *13*, 365–369. [CrossRef]
23. Lee, Y.; Kang, P.; Jung, S.; Bae, S.; Kim, J.; Lee, M.; Shin, D. Effect of carbon on the growth of TaC crystal derived from organometallic precursors. *J. Korean Ceram. Soc.* **2021**, *58*, 62–68. [CrossRef]
24. Ishizaka, T. Method of Plasma Enhanced Atomic Layer Deposition of TaC and TaCN Films Having Good Adhesion to Copper. US7407876B2, 5 August 2008. Available online: https://patents.google.com/patent/US7407876 (accessed on 20 April 2024).
25. Powell, C.F.; Campbell, I.E.; Gonser, B.W. The Deposition of Tantalum and Columbium from their Volatilized Halides. *J. Electrochem. Soc.* **1948**, *93*, 258–265. [CrossRef]
26. Kumar, S.; Mondal, S.; Kumar, A.; Ranjan, A.; Prasad, N.E. Chemical Vapor Deposition of TaC/SiC on Graphite Tube and Its Ablation and Microstructure Studies. *Coatings* **2017**, *7*, 101. [CrossRef]

27. Kondo, M. Tantalum Carbide-Coated Carbon Material and Manufacturing Method for Same. EP2520691A1, 7 November 2012. Available online: https://patents.google.com/patent/EP2520691A1 (accessed on 20 April 2024).
28. Levy, R.A. Investigation of Chemically Vapor Deposited Tantalum for Medium Caliber Gun Barrel Protection. SERDP Project WP-1425. 2008. Available online: https://www.serdp-estcp.org/Program-Areas/Weapons-Systems-and-Platforms/Surface-Engineering-and-Structural-Materials/Coatings/WP-1425/WP-1425#factsheet-5002-result (accessed on 20 April 2024).
29. Hoshino, Y.; Takeda, O.; Hoshi, M.; Sato, Y. Production of Tantalum Fine Powder by Reduction of Tantalum Chloride with Zinc Vapor. *ECS Trans.* **2009**, *33*, 247–253. [CrossRef]
30. Park, I.; Okabe, T.H.; Lee, O.; Lee, C.R.; Waseda, Y. Semi-Continuous Production of Tantalum Powder by Electronically Mediated Reaction (EMR). *Mater. Trans.* **2002**, *43*, 2080–2086. [CrossRef]
31. Goncharov, O.Y.; Treshchev, S.Y.; Ladyanov, V.I.; Faizullin, R.R.; Guskov, V.N.; Baldaev, L.K. Tantalum chemical vapor deposition on substrates from various materials. *Inorg. Mater.* **2017**, *53*, 1064–1068. [CrossRef]
32. Goncharov, O.Y.; Sapegina, I.V.; Faizullin, R.R.; Baldaev, L.K. Tantalum chemical vapor deposition on steel and tungsten substrates in the $TaBr_5$-Cd-He system. *Surf. Coat. Technol.* **2019**, *377*, 124893. [CrossRef]
33. Kalandarishvili, A.G.; Mikheev, V.K.; Chilingarishvili, P.D. Experimental Determination of the Saturated Vapor Pressure of Magnesium and Cadmium. *TVT* **1988**, *26*, 1016–1018.
34. Goncharov, O.Y. Thermodynamics of the Chemical Vapor Deposition of Carbides in the System $TaBr_5$–CCl_4–Cd. *Inorg. Mater.* **2001**, *37*, 237–242. [CrossRef]
35. Goncharov, O.Y.; Faizullin, R.R.; Guskov, V.N.; Baldaev, L.K. Equipment for chemical hydrogen-free gas-phase deposition of oxygen-free refractory materials. *News Acad. Eng. Sci. A. M. Prokhorov* **2015**, *4*, 3–9. Available online: https://elibrary.ru/item.asp?id=25051153 (accessed on 20 April 2024).
36. Goncharov, O.Y.; Faizullin, R.R.; Guskov, V.N.; Baldaev, L.K. Dispenser-Mixer. RU2640369, 22 December 2016. Available online: https://new.fips.ru/registers-doc-view/fips_servlet?DB=RUPAT&DocNumber=2640369&TypeFile=html (accessed on 20 April 2024).
37. Goncharov, O.Y.; Faizullin, R.R.; Guskov, V.N.; Baldaev, L.K. Dosing Saturator. RU158289, 22 May 2015. Available online: https://www1.fips.ru/fips_servl/fips_servlet?DB=RUPM&DocNumber=158289&TypeFile=html (accessed on 20 April 2024).
38. Goncharov, O.Y.; Faizullin, R.R.; Guskov, V.N.; Baldaev, L.K. Cassette Sample Feeder. RU173040, 8 August 2017. Available online: https://new.fips.ru/registers-doc-view/fips_servlet?DB=RUPM&DocNumber=173040&TypeFile=html (accessed on 20 April 2024).
39. Nefedov, V.I. *X-ray Photoelectron Spectroscopy of Chemical Compounds*; Khimiya: Moscow, Russia, 1984. (In Russian)
40. Morgan, D.J. Comments on the XPS Analysis of Carbon Materials. *C* **2021**, *7*, 51. [CrossRef]
41. Briggs, D.; Grant, J.T. (Eds.) *Surface Analysis by Auger and X-ray Photoelectron Spectroscopy*; IMPublications: Chichester, UK; SurfaceSpectra: Manchester, UK, 2003. [CrossRef]
42. Kim, H.M.; Shim, K.B.; Lee, J.M.; Lee, H.I.; Choi, K. Thermodynamic analysis on the chemical vapor deposition process of Ta-C-H-Cl system. *J. Ceram. Proces. Res.* **2018**, *19*, 519–524. [CrossRef]
43. Barna, P.B.; Adamik, M. Fundamental Structure Forming Phenomena of Polycrystalline Films and the Structure Zone Models. *Thin Solid Films* **1998**, *317*, 27–33. [CrossRef]
44. Fries, R.J.; Wahman, L.A. Effect of Stoichiometry on the Thermal Expansion of TaCx. *J. Am. Ceram. Soc.* **1967**, *50*, 475–477. [CrossRef]
45. Kumar, S.; Shekar, K.C.; Jana, B.; Manocha, L.M.; Prasad, N.E. C/C and C/SiC Composites for Aerospace Applications. In *Aerospace Materials and Material Technologies*; Part of the series Indian Institute of Metals Series; Springer: Singapore, 2016; pp. 343–369.
46. Loennberg, B. Thermal-expansion studies on the subcarbides of group V and VI transition metals. *J. Less-Comm. Met.* **1986**, *120*, 135–146. [CrossRef]
47. Shabalin, I.L. Molybdenum. In *Ultra-High Temperature Materials Vol 1*; Springer: Dordrecht, The Netherlands, 2014. [CrossRef]
48. Yu, R.K.; Kablov, E.N.; Kozlov, E.V.; Koneva, N.A.; Povarova, K.B.; Grabovetskaya, G.P.; Buntushkin, V.P.; Bazyleva, O.A.; Muboyadzhyan, S.A.; Budinovskii, S.A. *Struktura i Svoystva Intermetallidnykh Materialov s Nanofaznym Uprochneniyem (Structure and Properties of Intermetallic Materials with Nanophase Hardening)*; MISiS Publishing House: Moscow, Russia, 2008; 328p. (In Russian)
49. Kruglov, A.B.; Kruglov, V.B.; Osintsev, A.V. Measurement of the thermal coefficient of linear expansion on a speckle-interferometric dilatometer. *Instrum. Exp. Tech.* **2016**, *59*, 156–158. [CrossRef]
50. American Iron and Steel Institute. *High-Temperature Characteristics of Stainless Steel*. A Designers' Handbook Series No 9004; Toronto, Ont. Nickel Institute. 2020. Available online: https://nickelinstitute.org/media/4657/ni_aisi_9004_hightemperaturecharacteristics.pdf (accessed on 20 April 2024).
51. Miettinen, J. Thermodynamic assessment of Fe-Cr-Ni system with emphasis on the iron-rich corner. *Calphad* **1999**, *23*, 231–248. [CrossRef]
52. Clouet, E. Modeling of Nucleation Processes. In *ASM Handbook: Fundamentals of Modeling for Metals Processing*; ASM International 22A: Materials Park, OH, USA, 2009; pp. 203–219. Available online: http://emmanuel.clouet.free.fr/Articles/Clouet2009_ASM.pdf (accessed on 20 April 2024).

53. Mattsson, T.R.; Sandberg, N.; Armiento, R.; Mattsson, A.E. Quantifying the anomalous self-diffusion in molybdenum with first-principles simulations. *Phys. Rev. B* **2009**, *80*, 224104. [CrossRef]
54. Jena, A.K.; Chaturvedi, M.C. The role of alloying elements in the design of nickel-base superalloys. *J. Mater. Sci.* **1984**, *19*, 3121–3139. [CrossRef]
55. Maksimkin, O.P. Phase diffusionless γ-α transformations and their effect on physical, mechanical and corrosion properties of austenitic stainless steels irradiated with neutrons and charged particles. *IOP Conf. Ser. Mater. Sci. Eng.* **2016**, *130*, 012002. [CrossRef]
56. Kopas, P.; Blatnicky, M.; Sága, M.; Vasko, M. Identification of Mechanical Properties of Weld Joints of AlMgSi07.F25 Aluminium Alloy. *Metalurgija* **2017**, *56*, 99–102.
57. Rempel, A.A. Atomic and vacancy ordering in nonstoichiometric carbides. *Physics-Uspekhi* **1996**, *39*, 31–56. [CrossRef]